Magnetic phase switching driven by non-magnetic ion site disorder in pyrochlore $Yb_2(Ti_{1-x}Sn_x)_2O_7$

Zhiling Dun[1], Yunqi Cai[1], Chengkun Xing[2], Qi Cui[1], Naveen C. Muniraju[3], Emil S. Bozin[4], Jinguang Chenge[1,†], Haidong Zhou[2,‡]

[1]Institute of Physics, Chinese Academy of Sciences, Beijing 100190, China

[2]Department of Physics and Astronomy, University of Tennessee, Knoxville, TN 37996, USA

[3]Quantum Condensed Matter Division, Oak Ridge National Laboratory, Oak Ridge, TN 37831, USA

[4]Condensed Matter Physics and Materials Science Department

Brookhaven National Laboratory, Upton, NY, 11973, USA

* Email: jgcheng@iphy.ac.cn

‡ Email: hzhou10@utk.edu

May 31, 2022

While it is commonly accepted that the disorder on magnetic ion sites in quantum magnets usually generates a rugged free-energy landscape resulting in slow or glassy spin dynamics, the disorder effects on non-magnetic ion sites are still illusive. Here, using AC susceptibility measurements, we show that the mixture of Sn/Ti on the non-magnetic ion sites of pyrochlore $Yb_2(Ti_{1-x}Sn_x)_2O_7$ induces an antiferromagnetic ground state despite both parent compounds, $Yb_2Ti_2O_7$, and $Yb_2Sn_2O_7$, order ferromagnetically. This rare example demonstrates that the site disorder on non-magnetic ion sites could be a new path to achieve magnetic phase switching, which has been traditionally obtained by external stimuli such as temperature, magnetic field, pressure, strain, light etc.

Introduction

The quantum magnets are kept to be the focus of modern condensed matter physics studies since they provide unique opportunities not only to explore quantum many-body physics but also for applications of advanced technologies, such as spintronics and quantum computers. More attentions have recently been paid to their disorder effects since in reality, solid-state materials (maybe with the exception of silicon wafer) inevitably have defects and/or random disorder. The disorder effects due to aperiodically located magnetic moments are better understood. Electronically, such disorder on magnetic ion sites in a metallic system gives rise to the Kondo effect, for which the scattering between conduction electrons and impurity spins contributes a term to the electrical resistivity that increases logarithmically with lowering temperature [1]. Magnetically, depending on the level of dilution or vacancies, such disorder can either perturb spontaneous symmetry breaking and lead to a spin randomly oriented glassy state [2], or promote magnetic ordering and break a continuous degeneracy via an order by disorder mechanism [3]. Disorder can also coexist along with a well ordered magnetic sublattice since real materials usually contain non-magnetic ions that do not necessarily contain the same periodicity of the magnetic ions. How such disorder on non-magnetic ion sites impacts the quantum magnetism remains an open question with limited knowledge so far.

Two celebrated examples studied recently on this topic are $YbMgGaO_4$ (YMGO) and $Sr_2Cu\,(Te_{1-x}W_x)O_6$ (SCTWO). Both compounds are good insulators that feature a mixed-ion occupation on a non-magnetic sublattice. In YMGO, the Yb^{3+} ions with effective spin-1/2 moment form a geometrically frustrated triangular layer, between which is the site mixture of non-magnetic Mg^{2+}/Ga^{3+} ions. In SCTWO, the Cu^{2+} ions with spin-1/2 form a square layer with frustration arising from the competition between distinct types of exchange interactions. Though intriguing quantum spin liquid[4, 5, 6, 7, 8] like behaviors were suggested for both compounds by early studies [9, 10, 11, 12, 13, 14, 15, 16, 17], later experiments suggested an important role of non-magnetic ion site randomness[18, 19, 20, 21, 22, 23]. For YMGO, the Mg^{2+}/Ga^{3+} mixture strongly modifies the crystal field environment as well as its single ion magnetism [18], which might be related to the observed zero residual κ_0/T term on the thermal conductivity [19] and the frequency dependent AC susceptibility peak [20]. However, in a more recent thermal conductivity measurement, a non-zero κ_0/T term was observed which suggests that the quantum spin liquid state survives through the nonmagnetic site disorder [24]. For SCTWO, substituting W for Te alters the magnetic interactions from the strong nearest-neighbor type to the strong next-nearest-neighbor type [21], resulting in strong exchange interaction disorder that is absent in parent compounds Sr_2CuTeO_6 [25] and Sr_2CuWO_6 [26, 27]. Theoretically, one possible scenario proposed for both systems is the random-singlet (RS) state [22, 28, 29], in which the randomness in a quantum magnet can induce spin-singlet dimers of varying strengths with a spatially random manner and therefore account for the spin liquid like behaviors due to its widely distributed binding energy. Along with proposals for disorder-induced quantum spin liquids [17, 30, 31, 32, 33, 34, 35, 36, 37], the two examples mentioned above seems to suggest that disorder on the non-magnetic ion sites usually destroys magnetic orderings by promoting strong quantum spin fluctuations

(QSFs).

In this paper, we present a case that is drastically different, which is the pyrochlore $Yb_2(Ti_{1-x}Sn_x)_2O_7$ with the mixture of the non-magnetic Ti^{4+} and Sn^{4+} ions occupying the same crystallographic site. As a well-known geometrically frustrated magnet with the pyrochlore structure, $Yb_2Ti_2O_7$ has been extensively studied [38, 39, 40, 41, 42, 43, 44]. The most recent results on single crystals grown using traveling solvent floating zone method [45, 46, 47, 48] confirmed that it sits on a phase boundary between the splayed ferromagnetic (SF) phase and antiferromagnetic (AFM) Γ_5 phase from the SF side while containing significant volume fraction of short range AFM correlation within the ferromagnetic (FM) ground state. This coexistence could be due to that $Yb_2Ti_2O_7$ fluctuates in time between these two phases by quantum effects related to the strong QSFs of effective spin-1/2 Yb^{3+} ions or the AFM phase with a considerable fraction serves as domain walls between different SF domains [48]. Unlike SCTWO in which the two end members Sr_2CuTeO_6 and Sr_2CuWO_6 possess different magnetic ground states, $Yb_2Sn_2O_7$ shares the same low-temperature SF state as that of $Yb_2Ti_2O_7$ [49, 50]. Therefore, one does not expect the chemical pressure related to the lattice parameter change of $Yb_2(Ti_{1-x}Sn_x)_2O_7$ [50] will affect its magnetic ground state significantly. However, our results based on the AC susceptibility, neutron powder diffraction (NPD) and synchrotron x-ray diffraction (SXRD) measurements of $Yb_2(Ti_{1-x}Sn_x)_2O_7$ surprisingly show that an AFM ground state is induced in the Sn-doped samples without introducing extra structural distortion. Therefore, $Yb_2(Ti_{1-x}Sn_x)_2O_7$ represents a rare example demonstrating that the disorder on non-magnetic ion sites can serve as a new tool to tune/switch magnetic phases in quantum magnets, which is traditionally achieved via external stimuli such as temperature [51], magnetic field [52], pressure [53], strain [54], light [55] etc.

Results

Neutron and X-ray diffraction. For comparison, we synthesized both $Yb_2(Ti_{1-x}Sn_x)_2O_7$ and $Yb_2(Ti_{1-x}Ge_x)_2O_7$ samples and used NPD and SXRD to characterize their lattice structures. Fig. 1(a) shows the refinement for the NPD data of $Yb_2(Ti_{0.6}Sn_{0.4})_2O_7$ measured at room temperature using the POWGEN diffractometer. The data could be well fitted by the Fd-3m pyrochlore structure. The NPD data for several other Sn and Ge doped samples was also refined (not shown here), which all exhibits pure pyrochlore structure. As summarized in Fig. 1(c), the lattice parameter a decreases from $Yb_2Sn_2O_7$ to $Yb_2Ti_2O_7$ and then $Yb_2Ge_2O_7$ for all doped samples. This is reasonable since the lattice parameter is controlled by the ironic radius of the (Sn/Ti/Ge) site, and therefore the Sn sample has the largest lattice parameter, Ti sample has the second largest one, and Ge sample has the smallest one. We further used $\rho = d_{\text{Yb-O2}}/d_{\text{Yb-O1}}$ and the Yb-O2-Yb angle to characterize the axial distortion of the YbO_8 polyhedra, here $d_{\text{Yb-O1}}$ represents the bond length for the 6 longer Yb-O1 bonds in the plane perpendicular to the $< 111 >$ axis and $d_{\text{Yb-O2}}$ represents the bond length for the two shorter Yb-O2 bonds along the $< 111 >$ axis. As shown in Fig. 1(d), again, both of them decrease linearly.

Fig. 2(b) shows the SXRD pair distribution function data of $Yb_2(Ti_{0.5}Sn_{0.5})_2O_7$, G($r$), which is a Fourier

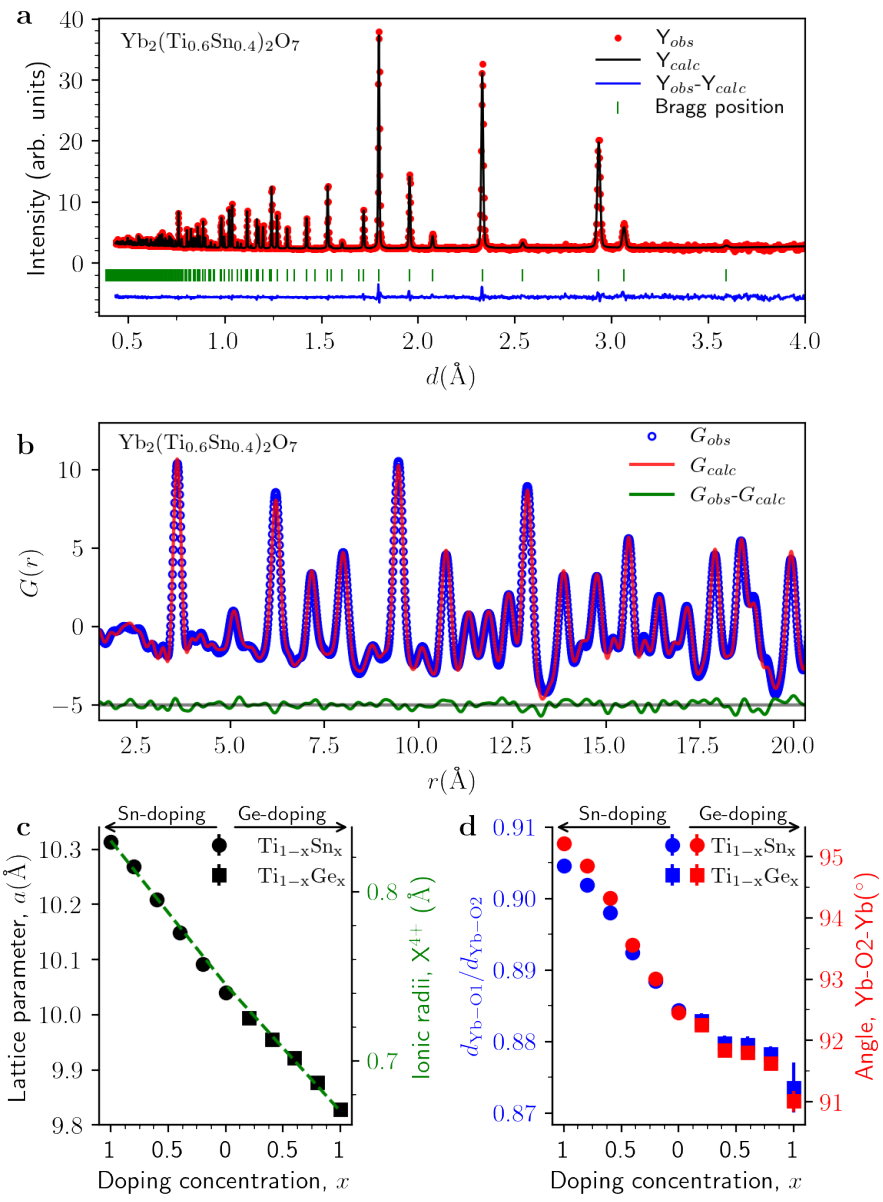

Figure 1: **Average and local structure of $Yb_2(Ti_{1-x}Sn_x)_2O_7$ and $Yb_2(Ti_{1-x}Ge_x)_2O_7$.** **a.** Neutron powder diffraction pattern (red circles) for $Yb_2(Ti_{0.6}Sn_{0.4})_2O_7$ measured at 300 K with wavelength 1.333Å at POWGEN. The solid black line is the refinement by using FULLPROF. Solid blue line at the bottom of the panel shows the difference between them. **b.** Pair distribution function, G(r), within the first two unit cell for 300 K $Yb_2(Ti_{0.6}Sn_{0.4})_2O_7$ data (blue circle). Best fit to G(r) using the average structure model and difference curve are shown in red and green lines, respectively. **c.** The doping concentration dependence of the lattice parameter as the average non-magnetic X^{4+} ionic radii. **d.** The doping level dependence of the ratio between the two different Yb-O bond lengths and the Yb-O2-Yb angle.

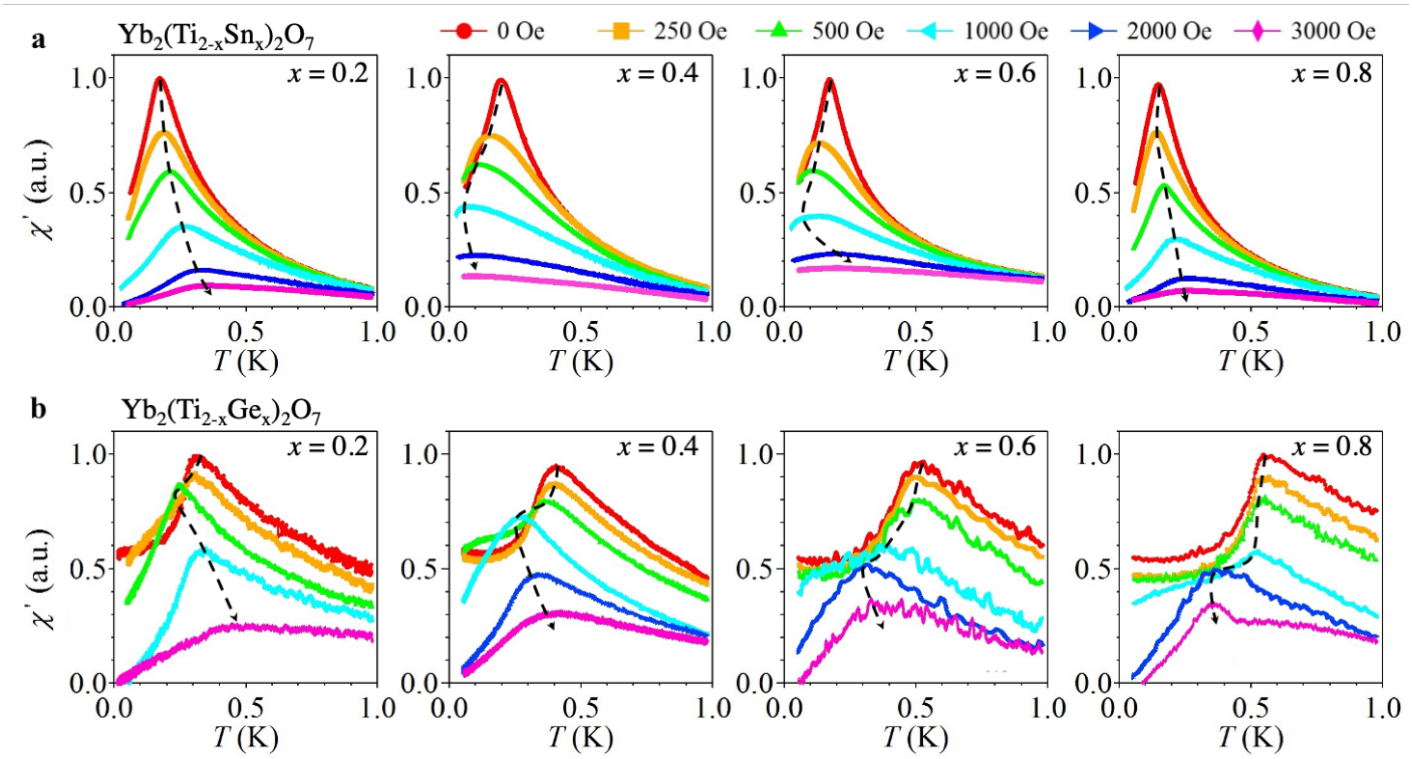

Figure 2: **AC susceptibility**. **a.** Real part of AC susceptibility measured under different DC magnetic fields for $Yb_2(Ti_{1-x}Sn_x)_2O_7$ with x = 0.2, 0.4, 0.6, and 0.8. **b.** Real part of AC susceptibility data for $Yb_2(Ti_{1-x}Ge_x)_2O_7$ with with x = 0.2, 0.4, 0.6, and 0.8. The used AC frequency is 3317 Hz for the Sn-doped system and 331 Hz for the Ge-doped system with a magnitude of 5 Oe. Dashed arrows indicate the evolution of the peak's position with increasing DC fields.

transform of the total scattering pattern. It measures the pair-pair correlations of atoms in real space, thus can reflect short-ranged structural order/distortion within short real space distance, r. Although the data lacks the sensitivity of first several Yb-O or Ti-O peaks due to the wiggles from Fourier transform, the general observation is that G(r) within the 1st unit cell can still be well-fitted by an average structural model of the pyrochlore lattice with randomly occupied Ti^{4+}/Sn^{4+} ions on the same site. Therefore, we conclude that the chemical disorder on non-magnetic ion sites does not introduce any noticeable local structural distortions in $Yb_2(Ti_{1-x}Sn_x)_2O_7$.

AC susceptibility. Fig. 2 shows the AC susceptibility measured at different DC magnetic fields for $Yb_2(Ti_{1-x}Sn_x)_2O_7$ and $Yb_2(Ti_{1-x}Ge_x)_2O_7$. For all samples, the data at zero field exhibits a peak, which represents the long range magnetic ordering at T*, which obviously shifts around under applied DC fields. As demonstrated in Ref. [50], the field dependence of AC susceptibility can be used as a convenient tool to identify the nature of a long-ranged magnetic ordering, i.e., the FM ordering temperature will shift to higher temperatures with increasing DC field due to the contribution of domain magnetization while the AFM ordering temperature will shows a negative DC field dependence.

The field dependence of T^* for each doping level was summarized in Fig. 3(a). The data shows (i) for $Yb_2Ti_2O_7$ and $Yb_2Sn_2O_7$, the T^* increases with increasing field, which is consistent with the fact that both samples have a SF ground state; (ii) for $Yb_2Ge_2O_7$, the T^* decreases with increasing field, which is consistent with its AFM ground state [50, 56, 57]; (iii) for all Sn and Ge-doped samples besides $Yb_2(Ti_{0.8}Sn_{0.2})_2O_7$, the T^* decreases first with increasing field and then increases while the field surpasses a critical value H_c. This indicates that as soon as Sn and Ge are doped, certain volume of AFM phase is introduced. This AFM order should be in long range nature since it dominates the bulk magnetism at low fields. With $H > H_c$, the sample comes back to ferromagnetic or is fully polarized; (iv) for $Yb_2(Ti_{0.8}Sn_{0.2})_2O_7$, it has ferromagnetic ground state since its T^* monotonically increases with increasing field.

Magnetic Phase Diagram. Accordingly, a magnetic phase diagram of T^* and H_c for $Yb_2(Ti_{1-x}Sn_x)_2O_7$ and $Yb_2(Ti_{1-x}Ge_x)_2O_7$ is summarized in Fig. 3(b). For Ge-doped samples, both T^* and H_c monotonically increase with increasing Ge-doping level. On the other hand, for Sn-doped samples, (i) while the T^* generally decreases with increasing Sn-doping level, it exhibits a dome around x = 0.5; (ii) the H_c first increases with increasing Sn-doping level, peaks at x = 0.5, and thereafter decreases.

The evolution of T^* and H_c in the Ge-doped samples is expected. The magnetic ground states of Yb-pyrochlores are decided by the ratio among the anisotropic exchange interactions [56, 58, 59]. Unlike $Yb_2Ti_2O_7$, $Yb_2Ge_2O_7$ orders antiferromagnetically in the Γ_5 manifold [57]. From the point view of chemical pressure effect, with increasing Ge-doping level in $Yb_2(Ti_{1-x}Ge_x)_2O_7$, the lattice parameter decreases monotonically and gradually tunes the balance of anisotropic exchanges interactions that drive the system towards the AFM Γ_5 phase from the SF phase side [56, 57]. Alternatively, if we assume that the phase coexistence in Ge-doped samples is similar to that of $Yb_2Ti_2O_7$, then the H_c could be scaled to the volume fraction of the AFM phase since the larger the H_c is, the more difficult to polarize the system. Therefore, the evolution of H_c in Fig. 3(b) means a monotonic increase in volume fraction of the AFM phase in $Yb_2(Ti_{1-x}Ge_x)_2O_7$, consistent with the SF and AFM phases in $Yb_2Ti_2O_7$ and $Yb_2Ge_2O_7$, respectively.

However, the appearance of the long range AFM order in $Yb_2(Ti_{1-x}Sn_x)_2O_7$ is surprising. Since both $Yb_2Ti_2O_7$ and $Yb_2Sn_2O_7$ have the SF ground state, an AFM ground state should not be expected for Sn-doped samples from the view of chemical pressure effects. Even if there is still magnetic phase coexistence [48], it is puzzling to observe this non-monotonic change of the volume fraction of AFM phase (or H_c in $Yb_2(Ti_{1-x}Sn_x)_2O_7$.

Discussion

The analysis above clearly shows that the disorder on non-magnetic ion sites must be involved in stabilizing the AFM order for $Yb_2(Ti_{1-x}Sn_x)_2O_7$. One possible scenario is that this disorder enhances the QSFs, which is similar to the cases of YMGO and SCTWO. With stronger QSFs, the $Yb_2(Ti_{1-x}Sn_x)_2O_7$ system possibly fluctuates to the AFM phase more frequently than to the SF phase and therefore shows dominating bulk AFM

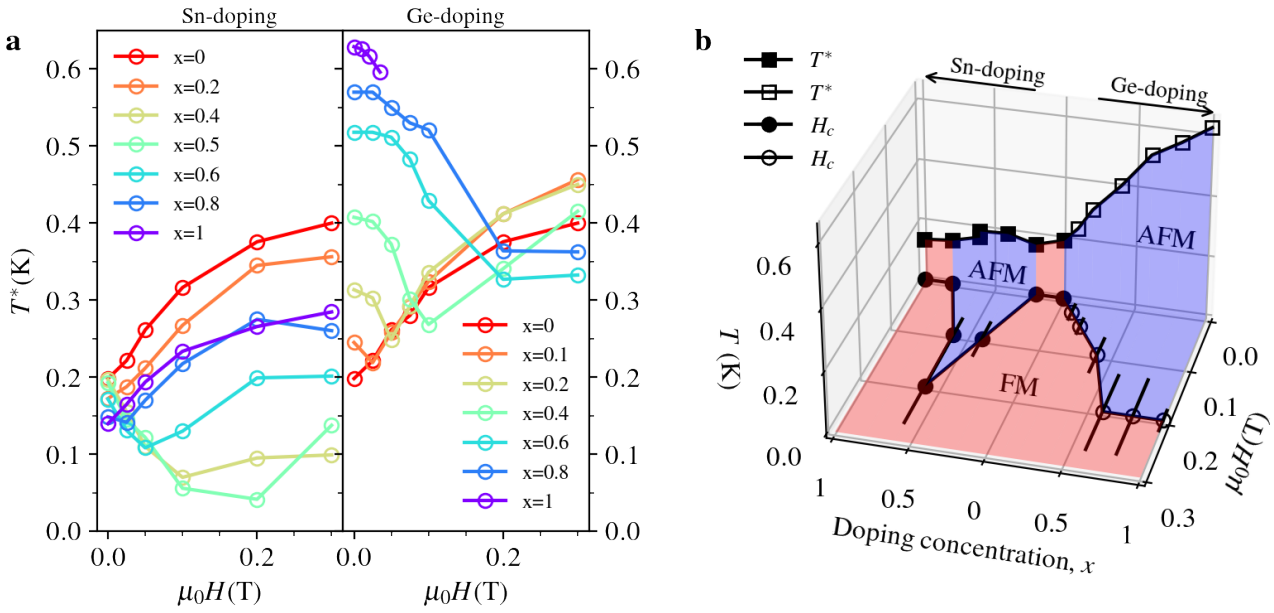

Figure 3: **Magnetic phase diagram. a.** The field dependence of the magnetic ordering temperature T* for $Yb_2(Ti_{1-x}Sn_x)_2O_7$ and $Yb_2(Ti_{1-x}Ge_x)_2O_7$ with different doping concentration. **b.** Magnetic phase diagram as a function of the doping concentration, x, temperature, T, and external DC field, $\mu_0 H$. Red and blue regions represent the FM and AFM phases, respectively. Data points for $Yb_2Ti_2O_7$, $Yb_2Sn_2O_7$, and $Yb_2Ge_2O_7$ are from Dun et al. [50].

behaviors at zero and low fields. This scenario is consistent with the fact that the doping dependence of the volume fraction of the AFM phase (the H_c) for $Yb_2(Ti_{1-x}Sn_x)_2O_7$ has a maximum at x = 0.5 that corresponds to the maximum site disorder. Another likely scenario is that this disorder introduces Yb-Yb exchange interaction randomness because the super-exchange path can be modified significantly with different orbital hybridization between O^{2-}(2p) and Ti^{4+} (empty 3d) or Sn^{4+} (empty 5p). Such randomness is not only found in YMGO and SCTWO, but also arises in other systems such as $Cr_2(Te_{1-x}W_x)O_6$ and Cr_2MoO_6 [60, 61]. Phenomenologically, the effect of exchange interaction randomness in frustrated magnets could be represented by an effective biquadratic exchange interaction with a positive sign [62], which usually prefers non-collinear or non-coplanar order. In this sense, if we attribute the phase coexistence in $Yb_2(Ti_{1-x}Sn_x)_2O_7$, it is likely that the AFM domain walls are energetically favored over the SF domain walls by the positive biquadratic exchange interactions since the SF state is mostly collinear, or the AFM domain walls are pinned to the local disorders. Then it naturally explains the more disorder, the more AFM phase fractions in $Yb_2(Ti_{1-x}Sn_x)_2O_7$ with the maximum AFM phase fraction occurring at x = 0.5.

Our results demonstrate the importance of the disorder effects on quantum magnets, even if the disorder is at the non-magnetic ion sites. Most surprisingly, We successfully achieved an AFM state by adding non-magnetic ion site disorder into ferromagnets. This finding provides a new route to achieve magnetic phase switching beyond the traditional stimuli. Since tuning and controlling magnetic phases is the key for magnetic materials research and potential technology applications, our finding here is expected to generate impacts on them.

Methods

Sample preparation. $Yb_2(Ti_{1-x}Sn_x)_2O_7$ were synthesized by standard solid state reaction. The stoichiometric amounts of Yb_2O_3, TiO_2, and SnO_2 were well mixed and annealed in air at 1400 degree for 24 hours. $Yb_2(Ti_{1-x}Ge_x)_2O_7$ were synthesized by high temperature high pressure technique. The appropriate amounts of Yb_2O_3, TiO_2, and GeO_2 were annealed under 7 GPa and 1000 degree by using a Walker-type multianvil module (Rockland Research Co.).

AC susceptibility The AC magnetic susceptibility measurement was carried out in a dilution refrigerator with the mutual induction method; an AC magnetic field of 5 Oe with a fixed frequency of 3317 Hz for Sn-doped samples and 331 Hz for Ge-doped samples was generated in the primary coil, and the output signal across two oppositely wound secondary coils was picked up with a Stanford Research SR830 lock-in amplifier.

Elastic neutron-scattering measurements. Elastic neutron-scattering experiments were performed on the POWGEN spectrometer at ORNL's SNS. Powder samples were loaded into vanadium cans and measured at room temperatures with with wavelength 1.333 Å.

Acknowledgments

Author contributions

Competing financial interests

The authors declare no competing financial interests.

Data Availability Statement

The data that support the plots within this paper and other findings of this study are available from the corresponding author upon reasonable request.

References

[1] Kondo J., Resistance minimum in dilute magnetic alloys. *Progress of Theoretical Physics* **32**, 37 (1964).

[2] Villain J., Insulating spin glasses. *Z. Phys. B* **33**, 31 (1979).

[3] Henley C. L., Ordering due to disorder in a frustrated vector antiferromagnet. *Phys. Rev. Letts.* **62**, 2056 (1989).

[4] Balents L., Spin liquids in frustrated magnets. *Nature* **464**, 199 (2010).

[5] Savary, L. & Balents, L. Quantum spin liquids: a review. *Rep. Prog. Phys.* **80**, 016502 (2016).

[6] Knolle, J. & Moessner, R. A field guide to spin liquids. *Annual Review of Condensed Matter Physics* **10**, 451-472 (2019).

[7] Zhou, Y., Kanoda, K. & Ng, T. K. Quantum spin liquid states. *Rev. Mod. Phys.* **89**, 025003 (2017).

[8] Broholm, C., Cava, R. J., Kivelson, S. A., NOCERA, D. G., NORMAN, M. R. & Senthil, T. Quantum spin liquids. *Science* **367**, eaayo668 (2020).

[9] Paddison, J. A. et al. Continuous excitations of the triangular-lattice quantum spin-liquid $YbMgGaO_4$. *Nat. Phys.* **13**, 117-122 (2017).

[10] Shen, Y. et al. Evidence for a spinon Fermi surface in a triangular lattice quantum-spin-liquid candidate. *Nature* **540**, 559-562 (2016).

[11] Li, Y. et al. Nearest-neighbour resonating valence bonds in $YbMgGaO_4$. *Nat. Commun.* 8, 15814 (2017).

[12] Shen, Y. et al. Fractionalized excitations in the partially magnetized spin liquid candidate $YbMgGaO_4$. *Nat. Commun.* **9**, 4138 (2018).

[13] Li, Y. et al. Gapless quantum spin liquid ground state in the two-dimensional spin-1/2 triangular antiferromagnet $YbMgGaO_4$. *Sci. Rep.* **5**, 16419 (2015).

[14] Li, Y. et al. Muon spin relaxation evidence for the U(1) quantum spin liquid ground state in the triangular antiferromagnet $YbMgGaO_4$. *Phys. Rev. Lett.* **117**, 097201 (2016).

[15] Li, Y. et al. Rearrangement of uncorrelated valence bonds evidenced by low-energy spin excitations in $YbMgGaO_4$. *Phys. Rev. Lett.* **122**, 137201 (2019).

[16] Mustonen, O. et al. Tuning the S=1/2 square-lattice antiferromagnet $Sr_2Cu(Te_{1-x}W_x)O_6$ from Néel order to quantum disorder to columnar order. *Phys. Rev. B* **98**, 064411 (2018).

[17] Mustonen, O. et al. Spin-liquid-like state in a spin-1/2 square-lattice antiferromagnet perovskite induced by d^{10}–d^0 cation mixing. *Nat. Commun.* **9**, 1085 (2018).

[18] Y. Li, et al., Crystalline electric-field randomness in the triangular lattice spin-liquid $YbMgGaO_4$. *Phys. Rev. Lett.* **118**, 107202 (2017).

[19] Xu, Y. et al. Absence of magnetic thermal conductivity in the quantum spin-liquid candidate $YbMgGaO_4$. *Phys. Rev. Lett.* **117**, 267202 (2016).

[20] Ma, Z. et al. Spin-glass ground state in a triangular-lattice compound $YbZnGaO_4$. *Phys. Rev. Lett.* **120**, 087201 (2018).

[21] Fogh E. et al., Randomness and frustration in a S = 1/2 square-lattice Heisenberg antiferromagnet. *ArXiv eprint*, arXiv:2112.03312 (2021).

[22] Hong, W. et al. Extreme suppression of antiferromagnetic order and critical scaling in a two-dimensional random quantum magnet. *Phys. Rev. Lett.* **126**, 037201 (2021).

[23] Watanabe, M. et al. Valence-bond-glass state with a singlet gap in the spin-1/2 square-lattice random J_1-J_2 Heisenberg antiferromagnet $Sr_2Cu(Te_{1-x}W_x)O_6$. *Phys. Rev. B* **98**, 054422 (2018).

[24] Rao, X. et al. Survival of itinerant excitations and quantum spin state transitions in $YbMgGaO_4$ with chemical disorder. *Nat. Commun.* bf 12, 4949 (2021).

[25] Koga, T. et al. Magnetic structure of the S = 1/2 quasi-two-dimensional square-lattice Heisenberg antiferromagnet Sr_2CuTeO_6. *Phys. Rev. B* **93**, 054426 (2016).

[26] Vasala, S. et al. Characterization of magnetic properties of Sr_2CuWO_6 and Sr_2CuMoO_6. *Phys. Rev. B* **89**, 134419 (2014).

[27] Vasala S. et al. Magnetic structure of Sr_2CuWO_6. *J. Phys.: Condens. Matter* **26** 496001 (2014).

[28] Kimchi, I., Nahum, A. & Senthil, T. Valence bonds in random quantum magnets: theory and application to $YbMgGaO_4$. *Phys. Rev. X* **8**, 031028 (2018).

[29] Ren, H. D., Xiong, T. Y., Wu, H. Q., Sheng, D. N., & Gong, S. S. Characterizing random-singlet state in two-dimensional frustrated quantum magnets and implications for the double perovskite $Sr_2CuTe_{1-x}W_xO_6$. *arXiv preprint* arXiv:2004.02128 (2021).

[30] Kawamura, H. & Uematsu, K. Nature of the randomness-induced quantum spin liquids in two dimensions. *J. Phys.: Condens. Matt.* **31**, 504003 (2019).

[31] Watanabe, K. et al. Quantum Spin-Liquid Behavior in the Spin-1/2 Random Heisenberg Antiferromagnet on the Triangular Lattice. *J. Phys. Soc. Jpn.* **83**, 034714 (2014).

[32] Shimokawa, T., Watanabe, K. & Kawamura, H. Static and dynamical spin correlations of the S = 1/2 random-bond antiferromagnetic Heisenberg model on the triangular and kagome lattices. *Phys. Rev. B* **92**, 134407 (2015).

[33] Uematsu, K., Kawamura, H. Randomness-Induced Quantum Spin Liquid Behavior in the S = 1/2 Random-Bond Heisenberg Antiferromagnet on the Pyrochlore Lattice. *Phys. Rev. Lett.* **123**, 087201 (2019).

[34] Hu, X. et al. Freezing of a Disorder Induced Spin Liquid with Strong Quantum Fluctuations. Phys. Rev. Lett. 127, 017201 (2021).

[35] Parker, E. & Balents, L. Finite-temperature behavior of a classical spin-orbit-coupled model for $YbMgGaO_4$ with and without bond disorder. *Phys. Rev. B* **97**, 184413 (2018).

[36] Bhatt, R. N. & Lee, P. A. Scaling studies of highly disordered spin-1/2 antiferromagnetic systems. *Phys. Rev. Lett.* **48**, 344-347 (1982).

[37] Kimchi, I. et al. Scaling and data collapse from local moments in frustrated disordered quantum spin systems. *Nat. Commun.* **9**, 4367 (2018).

[38] Rau, J. G. & Gingras, M. J. Frustrated quantum rare-earth pyrochlores. Annu. Rev. Condens. *Matter Phys.* **10**, 357–386 (2019).

[39] Pan, L. et al. Low-energy electrodynamics of novel spin excitations in the quantum spin ice $Yb_2Ti_2O_7$. *Nat. Commun.* **5**, 4970 (2014).

[40] Ross, K. A., Savary, L., Gaulin, B. D. & Balents, L. Quantum excitations in quantum spin ice. *Phys. Rev. X* **1**, 021002 (2011).

[41] Chang, L.-J. et al. Higgs transition from a magnetic Coulomb liquid to a ferromagnet in $Yb_2Ti_2O_7$. *Nat. Commun.* **3**, 992 (2012).

[42] Kermarrec, E. et al. Ground state selection under pressure in the quantum pyrochlore magnet $Yb_2Ti_2O_7$. *Nat. Commun.* **8**, 14810 (2017).

[43] Pan, L., Laurita, N. J., Ross, K. A., Gaulin, B. D. & Armitage, N. P. A measure of monopole inertia in the quantum spin ice $Yb_2Ti_2O_7$. *Nat. Phys.* **12**, 361–366 (2016).

[44] Tokiwa, Y. et al. Possible observation of highly itinerant quantum magnetic monopoles in the frustrated pyrochlore $Yb_2Ti_2O_7$. *Nat. Commun.* **7**, 10807 (2016).

[45] Arpino, K. E., Trump, B. A., Scheie, A. O., Mcqueen, T. M. & Koohpayeh, S. M. Impact of stoichiometry of $Yb_2Ti_2O_7$ on its physical properties. *Phys. Rev. B* **95**, 094407 (2017).

[46] Scheie, A. et al. Reentrant phase diagram of $Yb_2Ti_2O_7$ in a $\langle 111 \rangle$ magnetic field. *Phys. Rev. Lett.* **119**, 127201 (2017).

[47] Säubert, S. et al. Orientation dependence of the magnetic phase diagram of $Yb_2Ti_2O_7$. *Phys. Rev. B* **101**, 174434 (2020).

[48] Scheie, A. et al. Multiphase magnetism in $Yb_2Ti_2O_7$. *PNAS* **117**, 27245–27254 (2020).

[49] Yaouanc, A. et al. Dynamical splayed ferromagnetic ground state in the quantum spin ice $Yb_2Sn_2O_7$. *Phys. Rev. Lett.* **110,** 127207 (2013).

[50] Dun, Z. L. et al. Chemical pressure effects on magnetism in the quantum spin liquid candidates $Yb_2X_2O_7$ (X=Sn, Ti, Ge). *Phys. Rev. B* **89**, 064401 (2014).

[51] Spezzani, C. et al. Thermally induced magnetization switching in Fe/MnAs/GaAs(001): selectable magnetic configurations by temperature and field control. *Sci. Rep* **5**, 8120 (2015).

[52] Lin, G. et al. Field-induced quantum spin disordered state in spin-1/2 honeycomb magnet $Na_2Co_2TeO_6$. *Nat. Commun.* **12**, 5559 (2021).

[53] Hackl, A., Vojta, M. Pressure-induced magnetic transition and volume collapse in FeAs superconductors: an orbital-selective Mott scenario. *New J. Phys.* **11**, 055064 (2009).

[54] Zhang, H. et al. Comprehensive electrical control of metamagnetic transition of a quasi-2D antiferromagnet by in situ anisotropic strain. *Adv. Mater.* **32** 2002451 (2020).

[55] Baran, M. et al. Light-induced antiferromagnetic-ferromagnetic phase transition in $Pr_{0.6}La_{0.1}Ca_{0.3}MnO_3$ thin films. *Phys. Rev. B/*, **60** 9244–9247 (1999).

[56] Dun Z. L. et al. Antiferromagnetic order in the pyrochlores $R_2Ge_2O_7$ (R=Er, Yb). *Phys. Rev. B* **89**, 140407(R) (2015).

[57] Hallas, A. M. et al. XY antiferromagnetic ground state in the effective S = 1/2 pyrochlore $Yb_2Ge_2O_7$. *Phys. Rev. B* **93**, 104405 (2016).

[58] Taillefumier, M., Benton, O., Yan, H., Jaubert, L. D. C. & Shannon, N. Competing spin liquids and hidden spin-nematic order in spin ice with frustrated transverse exchange. *Phys. Rev. X* **7**, 041057 (2017).

[59] Wong, A. W. C., Hao, Z. & Gingras, M. J. P. Ground state phase diagram of generic XY pyrochlore magnets with quantum fluctuations. *Phys. Rev. B* **88**, 144402 (2013).

[60] Zhu M. et al. Tuning the magnetic exchange via a control of orbital hybridization in $\mathrm{Cr_2(Te_{1-x}W_x)O_6}$. *Phys. Rev. Lett.* **113**, 076406 (2014).

[61] Zhu M. et al. Ferromagnetic superexchange in insulating Cr_2MoO_6 by controlling orbital hybridization. *Phys. Rev. B* **92**, 094419 (2015).

[62] Smirnov A. I. et al. Order by Quenched Disorder in the Model Triangular Antiferromagnet $RbFe(MoO_4)_2$. *Phys. Rev. Lett.* **119**, 047204 (2017).